Percolating and nonpercolating liquid phase continuum model of drying in capillary porous media with application to solute transport in the very low Péclet number limit

Marouane Talbi and Marc Prat*
Institut de Mécanique des Fluides de Toulouse (IMFT), Université de Toulouse, CNRS, IMFT, Toulouse, France

(Received 31 May 2021; accepted 20 December 2021; published 14 January 2022)

A three equation continuum model of drying is presented. The model explicitly considers the liquid phase as formed by a percolating liquid phase and a nonpercolating liquid phase. The model is tested against pore network simulations. A quite good agreement is obtained between the predictions of the continuum model and data obtained by volume averaging the pore network simulation results. Then, the model is extended to the case where a solute is present in the liquid phase. This leads to the consideration of a five equation continuum model as opposed to the classically considered two equation model. The model is tested when diffusion is the solute dominant transport mechanism. In agreement with the pore network simulations, the five equation continuum model predicts that the solute concentration in the percolating liquid phase is greater than in the nonpercolating liquid phase in the considered situation. The work illustrates the key role of the liquid fragmentation process occurring during drying on the solute dynamics. Counterintuitively, although diffusion is dominant, it is shown that the solution concentration varies over the liquid phase as the result of the liquid phase fragmentation process.

DOI: 10.1103/PhysRevFluids.7.014306

I. INTRODUCTION

Drying in porous media is a topic a great interest with applications in chemical engineering [1], process engineering [2], food processing [3], civil engineering [4], and soil sciences [5], to name only a few. Its modeling and numerical simulation has a long history as reviewed in [6] or [7]. As presented in [6] and [7], the drying process in capillary porous media, defined as porous media with pores greater than about 1 μm in equivalent diameter, is commonly modeled within the framework of the continuum approach to porous media using a strongly nonlinear diffusion equation governing the evolution of the saturation in the medium [8]. However, this approach does not explicitly take into account an important feature of the drying process, namely the fact, sketched in Fig. 1, that the gradual replacement of the liquid by the gas phase in the pores resulting from the evaporation process leads to the fragmentation of the liquid phase into liquid clusters [9].

The fragmentation mechanism is inherent to the invasion percolation process [10] at the core of the drying process, e.g. [11]. One can refer to [12] for an illustration of the fragmentation process, i.e., the formation of a new cluster from an existing cluster as the result of a pore invasion. As discussed for instance in [9], one can distinguish a first period in the drying process, referred to as stage 1, where the liquid phase is distributed between the largest liquid cluster spanning the porous medium and a number of smaller clusters. The largest cluster is referred to as the main

*Corresponding author: mprat@imft.fr

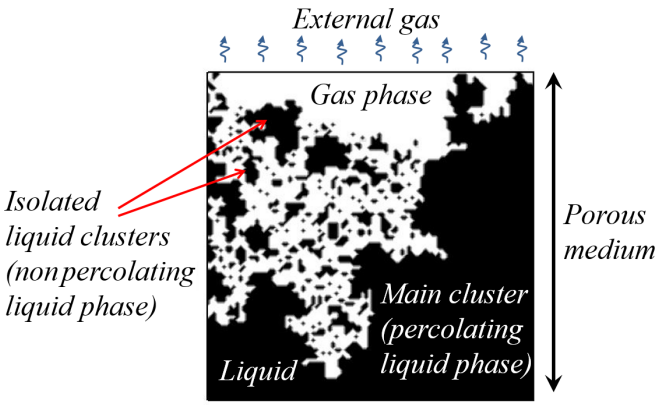

FIG. 1. Schematic of liquid phase fragmentation process during drying with main cluster (percolating liquid phase) and isolated clusters (nonpercolating liquid phase).

cluster whereas the smaller clusters are referred to as the isolated clusters. As shown in [13], this structuration of the liquid phase has an impact on the evolution of the spatial and temporal distribution of a dissolved species during drying. In other words, the question arises as to whether the liquid phase fragmentation process can be taken into account in the continuum approach to porous media so as to develop better models of the transport of a solute during drying. This holds true as well for other drying situations where particles are present in the liquid phase, e.g. [2,14]. To this end, we present in the current paper a three equation continuum model whose main variables are the vapor partial pressure, the main cluster saturation and the isolated clusters saturation. Regarding the liquid phase evolution, the three equation continuum model is based on the theory of biphasic flow in porous media presented in [15–18] proposing to treat microscopically percolating fluid regions differently from microscopically nonpercolating regions. With our definitions, the microscopically percolating liquid region corresponds to the main cluster whereas the isolated clusters correspond to the microscopically nonpercolating regions. As in a series of previous works [13,19–21], the method to discuss the relevance of the continuum model is to proceed via comparisons with simulations with a pore network model (PNM) of drying. However, since PNMs have been developed and a PNM is used here as a reference, one can wonder why continuum models are still worthy of interest. Due to computational issues, PNM simulations are actually limited to small networks. The largest network considered so far in drying PNM simulations is $80 \times 80 \times 80$ [22]. As reported in [22], the simulation of the full drying for a single realization required approximately 18 h on an Intel Xeon 3.6 GHz workstation. Simulations on larger networks require significantly more time (e.g., $100 \times 100 \times 100$ pore networks would require several days per realization [22]). As an example, consider a mean distance between pores of 10 μm. Then, a $100 \times 100 \times 100$ pore network would correspond to 1 mm^3 of porous medium. It is clear that in most applications the computational domain of interest is much larger. In other words, continuum models are usually the only option to deal with a drying situation of interest in the applications because of their much greater computational efficiency. As an illustration of this major difference in terms of computational efficiency between continuum models and PNM simulations, the continuum model solutions presented later in the paper are obtained from an Excel sheet in less than one second whereas the corresponding PNM simulations take a few days because the PNM results are averaged over several network realizations. Even when the spatial domain of interest is not very large, like in fuel cells for instance, e.g. [23,24], a full PNM approach is not possible due to the high pore size contrast between the various porous layers in the cell. Relying on continuum models is then again necessary either according to a full continuum approach, e.g. [25], or hybrid approaches combining PNM and continuum modeling, e.g. [23,24]. In brief, developing better continuum models is more than ever highly desirable due to

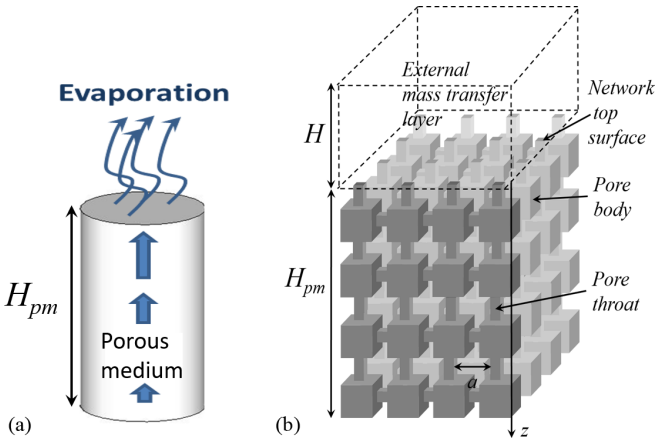

FIG. 2. (a) Basic drying situation referred to as macroscopically 1D drying. (b) Sketch of pore network representation with external diffusive layer on top.

their high computational efficiency and extending their capabilities is also highly desirable to deal with complex drying situations involving dissolved species and/or particles.

In the present paper, we consider the archetypical situation sketched in Fig. 2 where only the sample top surface is in contact with the external air. As an additional illustration of the computational efficiency issue between PNM and continuum model simulations, it can be noted that the continuum model formulation for the situation sketched in Fig. 2 is one dimensinal (1D) whereas the pore network simulations are 3D. We focus on the situations where the evaporation rate is sufficiently low for the temperature variations to be negligible. This situation is frequently encountered in the laboratory experiments with water at room temperature and referred to as "isothermal" drying. The corresponding drying process is often described in three main periods [26]: the constant rate period (CRP), the falling rate period (FRP), and the receding front period (RFP), but it is also usual to rather consider drying as a two stage process [27], with stage 1 corresponding to the CRP and stage 2 to the combination of the FPR and RFP. As in [13], we mainly focus on the period where the main cluster spans the porous sample, i.e., stage 1.

The paper is organized as follows: In Sec. II, the NLE two equation model is briefly recalled and the three equations continuum model is described. The drying PNM is summarized in Sec. III. Results of PNM simulations are presented in Sec. IV. A comparison between PNM results and the three equation continuum model solution is presented in Sec. V. The model is extended so as to consider the presence of a solute in Sec. VI where comparisons between the continuum model and PNM simulations are also presented. This is followed by Sec. VII which proposes a discussion. Section VIII consists of the main conclusions of the study.

II. CONTINUUM MODEL

A. NLE two equation continuum model

The nonlocal equilibrium (NLE) two-equation model is first recalled. As discussed in some detail in [19], the NLE two-equation model is preferred to the conventional approach, i.e. [8], for the following reason. The conventional approach is based on the use of the equilibrium desorption isotherm to relate the vapor partial pressure and the saturation whereas the impact of adsorption phenomena is presumably negligible in the relatively big pores of capillary porous media. This questionable aspect is circumvented by the NLE two equation model whose main variables are the

saturation and the vapor partial pressure and which does not rely on the desorption isotherm. As described in [21], the nonlocal equilibrium (NLE) two-equation model can be expressed as

$$\varepsilon \rho_l \frac{\partial S}{\partial t} + \nabla \cdot (\rho_l \mathbf{U}_l) = -\dot{m} \tag{1}$$

$$\nabla \cdot \left(\varepsilon (1 - S) D_{\text{eff}} \frac{M_v}{RT} \nabla P_v \right) + \dot{m} = 0, \tag{2}$$

where ε, t, D_{eff}, S, ρ_l, and P_v denote the porosity, time, effective vapor diffusivity, liquid saturation, water density, and water vapor partial pressure, respectively. M_v, R, and T represent the molar mass of water, universal gas constant, and temperature; $\dot{m}$ is the liquid-vapor phase change rate. The latter is also referred to as the NLE phase change term. As shown in [21], $\dot{m}$ can be expressed as

$$\dot{m} \approx -a_{gl} \frac{M_v}{RT} \beta (P_{vs} - P_v), \tag{3}$$

where a_{gl} is the specific interfacial area and β is a coefficient; P_{vs} is the saturation vapor pressure since adsorption phenomena are not considered.

B. Three equation continuum model

The main difference with the three equation model is to explicitly consider that the liquid phase can be split in the percolating liquid phase, also referred to as the main cluster, and the nonpercolating liquid phase. In the three equation model, the liquid saturation is thus expressed as

$$S = S_1 + S_2, \tag{4}$$

where the subscript 1 is for the percolating liquid phase, i.e., the main cluster, and the subscript 2 is for the nonpercolating liquid phase, i.e., the isolated clusters. Subscript 3 refers to the vapor (the gas phase is a binary gas formed by air and the vapor of the evaporating species).

Assuming a homogeneous porous medium, mass balance equations for the percolating and nonpercolating liquid phases are expressed as

$$\varepsilon \rho_l \frac{\partial S_1}{\partial t} + \nabla \cdot (\rho_l \mathbf{U}_{l1}) = -\dot{m}_{12} - \dot{m}_{13}, \tag{5}$$

$$\varepsilon \rho_l \frac{\partial S_2}{\partial t} + \nabla \cdot (\rho_l \mathbf{U}_{l2}) = -\dot{m}_{21} - \dot{m}_{23}, \tag{6}$$

where ε is the porous medium porosity, ρ_l is the liquid density, $\mathbf{U}_{l1}$ is the filtration velocity in the percolating liquid phase, $\mathbf{U}_{l2}$ is the filtration velocity in the nonpercolating liquid phase, $\dot{m}_{12}$ is the mass transfer rate between phase 1 and phase 2, $\dot{m}_{13}$ is the evaporation rate of phase 1 per unit volume of porous medium, $\dot{m}_{21}$ is the mass transfer rate between phase 2 and phase 1, and $\dot{m}_{23}$ is the evaporation rate of phase 2 per unit volume of porous medium. Since a new isolated cluster actually forms as the result of the fragmentation of the main cluster, we also have

$$\dot{m}_{12} = -\dot{m}_{21}. \tag{7}$$

It can be noted that in isothermal drying an isolated cluster cannot reconnect to the main cluster, hence $\dot{m}_{12} > 0$.

The gas phase forms a single cluster in the drying process. The mass conservation of the vapor is expressed as for the NLE two equation continuum model, i.e., Eq. (2),

$$\nabla \cdot \left(\varepsilon (1 - S) D_{\text{eff}} \frac{M_v}{RT} \nabla P_v \right) + \dot{m} = 0, \tag{8}$$

where

$$\dot{m} = \dot{m}_{13} + \dot{m}_{23}. \tag{9}$$

The phase change rate is expressed as for the NLE two equation continuum model as

$$\dot{m} = a_{lg}\beta\frac{M_v}{RT}(P_{vs} - P_v) \tag{10}$$

with

$$\dot{m}_{13} = a_{l1g}\beta\frac{M_v}{RT}(P_{vs} - P_v), \tag{11}$$

$$\dot{m}_{23} = a_{l2g}\beta\frac{M_v}{RT}(P_{vs} - P_v), \tag{12}$$

where a_{l1g} (a_{l2g} respectively) is the specific interfacial area between phase 1 (phase 2 respectively) and the gas phase. It can be noted that $a_{lg} = a_{l1g} + a_{l2g}$.

Following [18], the mass transfer rate $\dot{m}_{12}$ between the percolating and nonpercolating liquid phases is expressed as

$$-\dot{m}_{12} = \eta\varepsilon\rho_l\left(\frac{S_2 - S_{irr}}{S_{irr} - S}\right)\frac{\partial S}{\partial t}, \tag{13}$$

where η is a numerical factor, S_{irr} is the irreducible saturation. Equation (13) represents the continuum modeling of the fragmentation process. It expresses that the occurrence of new clusters from the main cluster is proportional to the liquid phase saturation variation rate whereas the factor $(\frac{S_2 - S_{\text{irr}}}{S_{\text{irr}} - S})$ is qualitatively consistent with the fact that the closer the system is to the irreducible saturation, the greater is the probability to form a new cluster from the main cluster since the main cluster structure becomes increasingly ramified as the irreducible saturation is approached [10]. This functional form is qualitatively consistent with the nonlinear increasing variation of the number of clusters during the drying process [9] (also illustrated in Fig. 4 below from PNM simulations). As we shall see, it also leads to quantitatively consistent results.

The above model is simplified by introducing additional assumptions. The flow in the percolating phase is modeled using the generalized Darcy's law,

$$\mathbf{U}_{l1} = -\frac{kk_{r1}}{\mu}\nabla P_{l1}, \tag{14}$$

where $\mathbf{U}_{l1}$ is the percolating liquid phase filtration velocity, P_{l1} is the pressure in the percolating liquid phase, k is the medium permeability, k_{r1} is the percolating phase relative permeability, and μ is the liquid viscosity. By introducing the capillary pressure curve $P_{c1}(S_1)$, where $P_{c1}(S_1)$ is the local pressure difference between the gas phase and the percolating liquid phase, Eq. (5) can be expressed as

$$\varepsilon\rho_l\frac{\partial S_1}{\partial t} + \nabla\cdot(\rho_l D_{l1}(\mathrm{S}_1)\nabla S_1) = -\dot{m}_{12} - \dot{m}_{13}, \tag{15}$$

where

$$D_{l1}(\mathrm{S}_1) = -\frac{kk_{r1}}{\mu}\frac{dP_{c1}}{ds_1}. \tag{16}$$

The nonpercolating liquid phase is assumed immobile. Equation (6) is thus simplified as

$$\varepsilon\rho_l\frac{\partial S_2}{\partial t} = -\dot{m}_{21} - \dot{m}_{23}. \tag{17}$$

C. Boundary conditions

For the 1D case sketched in Fig. 2(a), the boundary conditions at the bottom read

$$-\rho_l D_{l1}(S_1)\nabla S_1 \cdot \mathbf{n} = 0 \tag{18}$$

and

$$-\varepsilon(1-S)D_{\text{eff}}\frac{M_v}{RT}\nabla P_v \cdot \mathbf{n} = 0, \tag{19}$$

where $\mathbf{n}$ is a unit normal vector to the considered surface.

The definition of the boundary conditions at the top surface is still a debated question in the drying theory [21,28–30]. In other words, the coupling at the surface between the transport phenomena in the porous medium and in the external air in contact with the porous medium surface is not yet sufficiently well understood and modeled. In the case of the three equation continuum model, the detailed modeling of the mass transfer at the top surface is particularly challenging since one has to consider that the vapor leaves the porous medium surface from three categories of pores: (i) by evaporation from liquid filled pores belonging to the main cluster (percolating liquid phase), (ii) by evaporation from liquid filled pores belonging to isolated clusters connected to the surface (nonpercolating liquid phase), and (iii) gaseous pores. However, this challenging modeling issue is left for a future work. In the present study, the focus is on the modeling of the liquid phase internal fragmentation. A simplified approach is therefore adopted. As explained in more detail later in the paper, this simplified approach consists in assuming that the overall evaporation rate is input data for the model and not an outcome.

D. Macroscopic parameters

As can be seen from the above, the use of the three equation continuum model implies in general to specify several parameters, most of them being nonlinear functions of saturation. However, the focus in this paper is on the liquid phase fragmentation process, which is taken into account in the three equation continuum model via Eq. (13). For this reason, a particular drying regime is considered (as explained in the next section). The consideration of this particular regime allows focusing on $\dot{m}_{12}$ [Eq. (13)] without the need to determine the many other parameters of the three-equation continuum model. Nevertheless, the complete model was presented for the readers interested in more complex situations requiring the consideration of the full set of equations.

III. PORE NETWORK MODEL

As in [9], a simple cubic network is considered [Fig. 2(b)]. The distance between two adjacent nodes in the network is the lattice spacing, denoted by a. In this model, the pore bodies located at the nodes of the cubic grid are cubes of size d_p with d_p varying in the range [0.675, 0.725] according to a uniform probability distribution function, noting that the lengths in the PNM are made dimensionless using the lattice spacing a as reference length. The pore throats are channels connecting the pore bodies. The throat size d_t is distributed in the range [0.075, 0.125] according to a uniform distribution law. The drying algorithm is the one presented in [11]. As discussed in [31,32] or [33] this algorithm applies to the isothermal drying situation where capillary effects are dominant and corner film flows [34,35] can be neglected. The interested readers can refer to the afore-mentioned articles for details on the algorithm and additional information on the pore network modeling of the drying process.

It must be recalled that that the viscous effects are not explicitly considered in the liquid phase in the version of the algorithm considered in the present paper. As discussed in [31], various drying regimes can be actually distinguished depending on the competition between the capillary forces, the gravity, and the viscous forces. Here, the capillarity dominant regime is considered. Both the effects of gravity and the viscous forces are assumed to be negligible compared to the capillarity. This

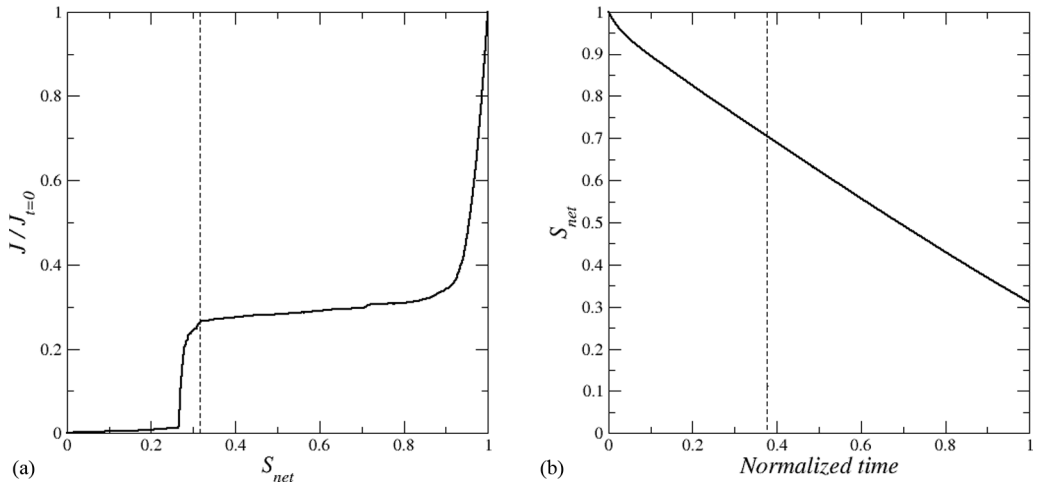

FIG. 3. Evolution of (a) the evaporation rate (drying curve); the vertical dashed line indicates the end of stage 1, (b) the overall network liquid saturation S_{net} in the range [0.31–1]. The reference time is the time when $S_{\text{net}} = 0.31$, which corresponds to the end of stage 1. The vertical line corresponds to $S_{\text{net}} = 0.7$, which is the maximum saturation considered for the comparison with the continuum model (see text).

regime is referred to as the capillary regime. As a matter of fact, the special case when the viscous effects can be neglected compared to the capillary effects even when the main cluster becomes very ramified as the irreducible saturation is approached is considered. For this reason, this regime is referred to as the "asymptotic" capillary regime. Additional details on this regime are given later in the paper.

IV. PORE NETWORK SIMULATIONS

PNM simulations of the drying process were performed with a $N \times N \times N$ cubic network, where N is the number of nodes in the network along each direction of a 3D Cartesian coordinate system [$N = 4$ for the network sketched in Fig. 2(b)]. The results presented in what follows were obtained for $N = 30$. The external boundary layer thickness [denoted by H in Fig. 2(b)] was 10.

Figure 3(a) shows the variation of the computed evaporation rate (normalized by the evaporation rate at $t = 0$) as a function of S_{net}, i.e., the overall network liquid saturation. Note that these data as well as the other PNM data presented in the paper are averages over 15 realizations of the network unless otherwise mentioned. The classical evolution [26,27] is retrieved with a first period, referred to as stage 1, in which the evaporation rate varies weakly over a significant range of saturations (corresponding to S_{net} varying between about 0.8 and 0.31). This period is referred to as stage 1. As can be seen in Fig. 3(a), stage 1 ends when S_{net} is about equal to 0.31, which corresponds to the vertical dashed line in Fig. 3(a). Then the evaporation rate drops. This corresponds to stage 2. However, contrary to the classical experimental results [26], an initial period where the evaporation rate drops can be observed before the quasiconstant rate period starts in stage 1 [this approximately corresponds to S_{net} in the range [0.9–1] in Fig. 3(a)]. This period is discussed below with the results on the saturation profiles. Figure 3(b) shows the evolution of S_{net} as a function of time. The reference time is the time when $S_{\text{net}} = 0.31$ ($t_{\text{ref}}. = t_{S\text{net}=0.31}$). Since the focus on what follows is stage 1, the evolution of S_{net} in Fig. 3(b) is shown down to $S_{\text{net}} = 0.31$. Consistently with the variation of the evaporation rate in Fig. 3(a), the evolution of S_{net} shows an initial period where S_{net} decreases faster compared with the longer period that follows where the slope of the curve in Fig. 3(b) is smaller and varies weakly.

Figure 4 illustrates the liquid phase fragmentation process occurring during the drying process. As can be seen, the number of liquid clusters increases during stage 1. The liquid phase is actually

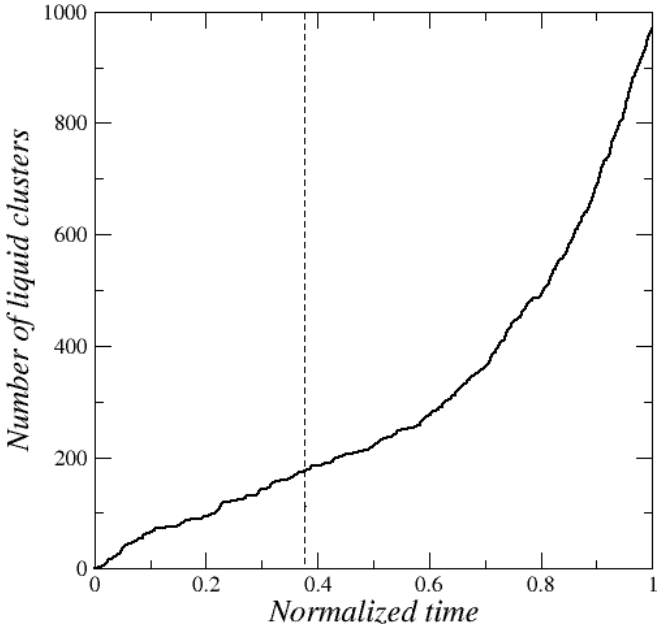

FIG. 4. Number of liquid clusters in the network as a function of time up to the end of stage 1. The vertical line corresponds to $S_{\text{net}} = 0.7$.

formed during stage 1 by a main or percolating cluster and an increasing number of isolated or nonpercolating clusters.

Saturation profiles during the drying process up to the end of stage 1 are depicted in Fig. 5. These profiles are averages over horizontal slices, i.e., transverse to the z direction, according to a procedure similar to the one used in previous works [19,20,21]. The slices are ten lattice spacing thick in the present work.

This choice is motivated by the fact that the computations of macroscopic parameters from PNM simulations, such as for instance the local porosity as illustrated in Fig. 6, indicate that an averaging volume of size $10a$ can be considered as a reasonable representative elementary volume (REV). Thus a running averaging procedure is used considering slices of size $N \times N \times 10$. The computed values are affected to the center of the slices. It can be also noted that slice saturations are actually typically considered in the experiments [36,37]. The selected slice thickness explains why the profiles start at $z = 5$ (in lattice spacing unit) and ends at $z = 25$ in Fig. 5. The slice averaged saturations are denoted by S_{sl}, $S_{1\text{sl}}$, and $S_{2\text{sl}}$, respectively.

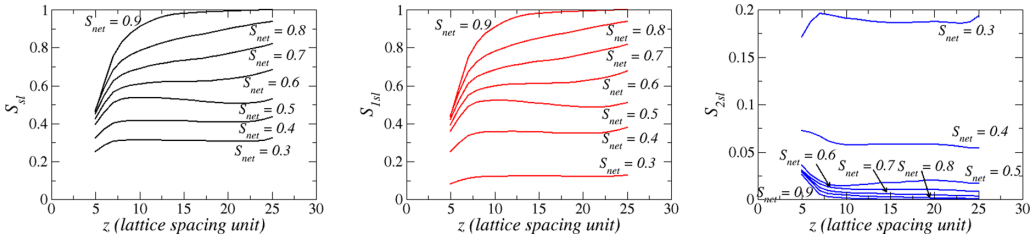

FIG. 5. Liquid phase saturation profiles (S_{sl}), percolating liquid phase ($S_{1\text{sl}}$), and nonpercolating liquid phase ($S_{2\text{sl}}$) saturation profiles (corresponding to $S_{\text{net}} = 0.9, 0.8, 0.7, 0.6, 0.5, 0.4, 0.3$); $z = 0$ corresponds to the network top surface [Fig. 2(b)] whereas $z = 30$ to the network bottom limiting surface.

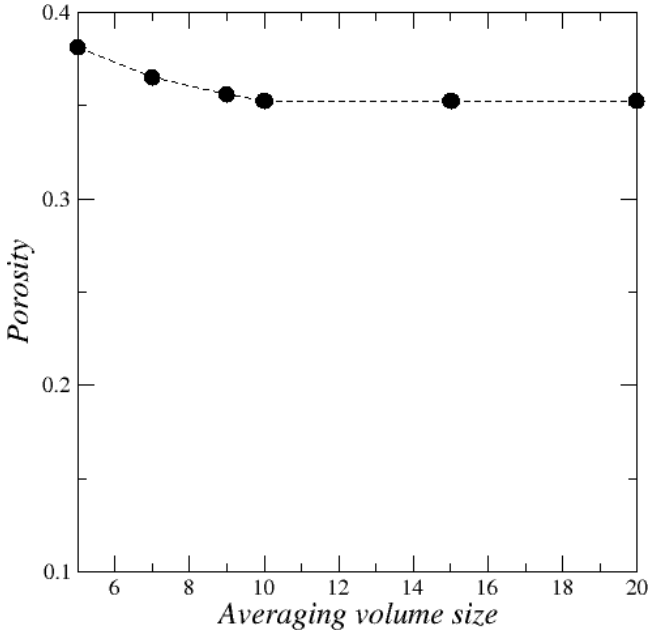

FIG. 6. Porosity variation as a function of averaging volume size obtained by computing the porosity over a cubic volume of increasing size located within the network.

The liquid phase saturation profiles in Fig. 5 present several differences compared to the profiles typically obtained in the experiments. For the capillary regime considered in the present paper, the latter are typically flat, e.g., [36,37]. By contrast, edge effects are noticeable at both ends of each profile in Fig. 5. The profiles are flat only in the region away from the edges. Also, they become flat in this region only when S_{net} is sufficiently low, i.e., when $S_{\text{net}} \sim 0.6$–0.7. These differences with the experimental profiles are discussed in detail in [30]. The initial period where the profiles are not flat in the central region is associated with a finite size effect and corresponds to the period where S_{net} varies from 1 to S_{BT}, where S_{BT} is the saturation at breakthrough. Since the saturation at breakthrough, i.e., when the gas phase reaches for the first time the network bottom, scales as $1 - S_{\text{BT}} \propto N^{-\alpha}$ where $\alpha = 0.48$ in three dimensions according to the percolation theory [10,38], this initial period becomes negligible for a sufficiently large network, and thus cannot be seen typically in the experiments. By contrast, the edge effect size is found to be independent of the network size and on the order of a few lattice spacing [30].

As a result, the corresponding variations of the saturation in the edge regions is indiscernible in the experiments since the size of the edge effect regions is typically very small compared to the sample size in the experiments. For these reasons, the main objective of continuum models as regards the saturation profiles should be to predict the flat profile evolutions since the finite size effect impacted period is negligible in most experiments as well as the relative extension of the edge effect regions. For the sake of comparison with the continuum model, we therefore consider as main targets S_{bulk}, $S_{1\,\text{bulk}}$, and $S_{2\,\text{bulk}}$ where S_{bulk}, $S_{1\,\text{bulk}}$, and $S_{2\,\text{bulk}}$ are the values of S_{sl}, $S_{1\text{sl}}$, and $S_{2\text{sl}}$ in the middle of the network, i.e., at $z = 16$ in Fig. 5.

The variations of S_{bulk}, $S_{1\,\text{bulk}}$, and $S_{2\,\text{bulk}}$ are depicted in Fig. 7. The variations are shown over the period corresponding to S_{net} in the range [0.3, 0.7] which is defined as the period of interest. From the above data, the period of interest in what follows is defined as the period of stage 1 not affected by the finite size effect. It approximately corresponds to the range of overall saturation [0.3–0.7] for the considered network. As illustrated in Fig. 5, the saturation profiles in the bulk are reasonably flat for $S_{\text{net}} < 0.7$.

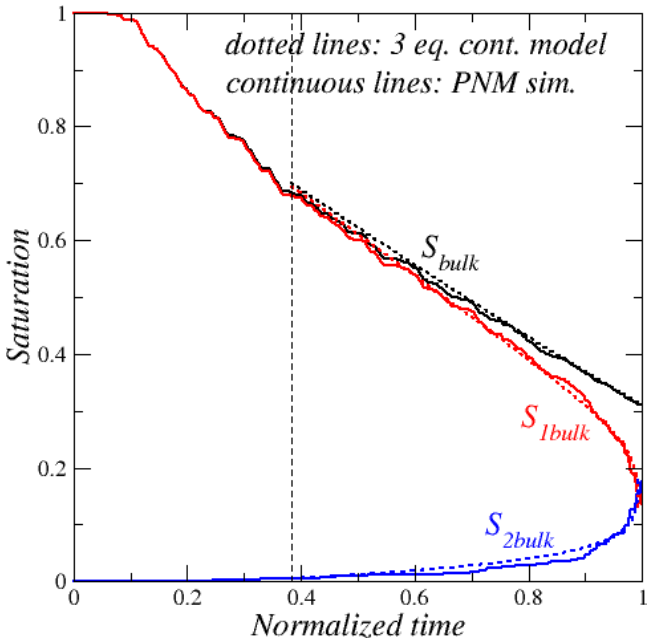

FIG. 7. Variation of S_{bulk}, $S_{1\,\text{bulk}}$, and $S_{2\,\text{bulk}}$ as a function of time during stage 1. Comparison between the PNM data and the results from the three equation continuum model. The comparison is performed for overall saturations lower than 0.7 for the comparison to not be hampered by the initial significant finite size effect (see text). The overall saturation 0.7 corresponds to the vertical dashed line in the figure.

As can be seen, the percolating phase saturation decreases over stage 1 whereas the nonpercolating liquid phase saturation increases. The variations of both saturation are much faster and more important as the end of stage 1 is approached. As discussed in [9], the end of stage 1 corresponds to the situation when the percolating liquid phase is about to cease percolating. In the considered asymptotic capillary regime, this corresponds to the situation when the irreducible saturation is about to be reached. From Fig. 3(a), it can therefore be considered that $S_{\text{irr}} \approx 0.31$.

V. CONTINUUM MODEL SOLUTION

In order to solve the three equation continuum model, Eqs. (4)–(17), the following parameters must be in principle determined: ε, $D_{\text{eff}}(S)$, a_{l1g}, a_{l2g}, β, η, S_{irr}, k, k_{r1}, $P_{c1}(S_1)$ noting that the parameters D_{eff}, a_{l1g}, a_{l2g}, k_{r1}, P_{c1} are nonlinear functions of the saturation. As exemplified in [19,21,39], these parameters can be determined from PNM simulations. Also, because of the nonlinearity, Eqs. (4)–(17) must be generally solved using a numerical method. However, it can be observed from Fig. 5 that the profiles are spatially uniform (when as discussed before the edge effects are not taken into consideration and the initial period affected by the finite size effect is discarded). Under these circumstances, the numerical solution can be greatly simplified and the determination of most of the three equation continuum model parameters from specific PNM numerical simulations can be avoided. In [30], it is shown that S_{bulk} can be determined from the following equation:

$$\varepsilon \rho_l H_{\text{pm}} \frac{\partial S_{\text{bulk}}}{\partial t} = -j, \tag{20}$$

where j is the evaporation flux and H_{pm} is the porous medium height (Fig. 2).

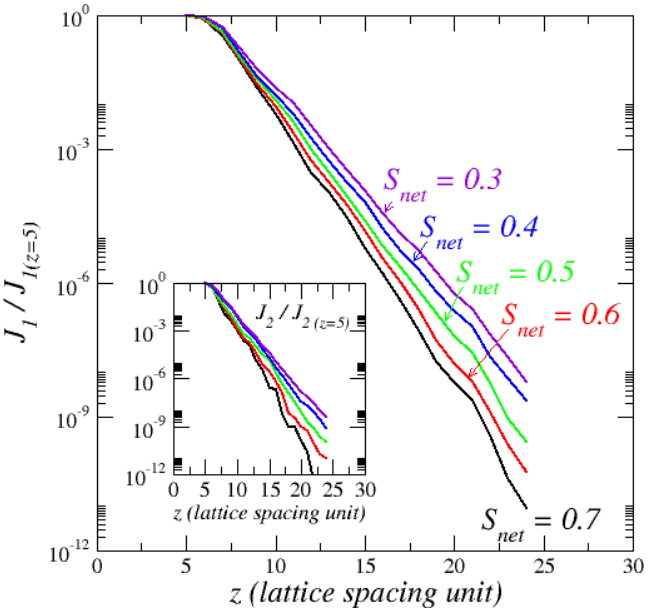

FIG. 8. Variation of evaporation rate from percolating cluster (J_1) and nonpercolating clusters (J_2) in the slices as a function of z for various network saturations (the colors in the inset corresponds to the same overall saturations as in the main figure).

Since $S_{\text{bulk}} = S_{1\,\text{bulk}} + S_{2\,\text{bulk}}$, one obtains from Eq. (20)

$$\varepsilon \rho_l H_{\text{pm}} \frac{\partial S_{1\,\text{bulk}}}{\partial t} = -j - \varepsilon \rho_l H_{\text{pm}} \frac{\partial S_{2\,\text{bulk}}}{\partial t}. \tag{21}$$

The governing equation for S_2, namely Eq. (17), can be simplified in the bulk as

$$\varepsilon \rho_l \frac{\partial S_{2\,\text{bulk}}}{\partial t} = -\dot{m}_{21} \tag{22}$$

because, as illustrated in Fig. 8, the liquid-vapor phase change is negligible in the network outside the top edge effect region. This leads to expressing Eq. (21) as

$$\varepsilon \rho_l \frac{\partial S_{1\,\text{bulk}}}{\partial t} = -\frac{j}{H_{\text{pm}}} + \dot{m}_{21}, \tag{23}$$

where, as mentioned before, it is proposed to express $\dot{m}_{21}$ as

$$\dot{m}_{21} = -\dot{m}_{12} = \eta \varepsilon \rho_l \left(\frac{S_{2\,\text{bulk}} - S_{\text{irr}}}{S_{\text{irr}} - S_{\text{bulk}}} \right) \frac{\partial S_{\text{bulk}}}{\partial t}. \tag{24}$$

We have tested Eqs. (22)–(24) from the PNM data. Equations (22) and (23) together with Eq. (24) were solved using a first order finite difference scheme to express the derivatives with respect to time, i.e., expressions of the form $\frac{\partial S_{2\,\text{bulk}}}{\partial t} = \frac{S_{2\,\text{bulk}}(t+\delta t) - S_{2\,\text{bulk}}(t)}{\delta t}$. The method was explicit, i.e., the values of the saturations involved in the expression of the source term $\dot{m}_{12}$ were taken at the previous time step. The saturation S_{bulk} was obtained from $S_{\text{bulk}} = S_{1\,\text{bulk}} + S_{2\,\text{bulk}}$. Since the initial period affected by the finite size effect is not considered, the simulations started with the following initial conditions imported from the PNM simulations: $S_{\text{bulk}} = 0.6833$, $S_{1\,\text{bulk}} = 0.678$, $S_{2\,\text{bulk}} = 0.005\,11$. Since the focus is on the evolution of the percolating and nonpercolating phases, the evaporation rate was considered as input data. Thus, the evaporation flux j computed from the PNM simulations was

used. This led to the results depicted in Fig. 7, which were obtained with $\eta = 0.1$ and $S_{\text{irr}} = 0.3138$. As can be seen, the three equation continuum model leads to a quite reasonable agreement with the PNM data. This is an interesting confirmation in the context of drying of the approach proposed in [18].

VI. SOLUTE CONCENTRATION EVOLUTION IN THE HYPERDIFFUSIVE LIMIT

As pointed out in [13] or in [40], the evolution of the concentration of a solute in a drying porous medium generally results from two main effects: (i) the solute convective transport in the percolating liquid phase which leads to the accumulation of solute in the porous medium top surface region (for the configuration depicted in Fig. 2), (ii) the fact that the volume occupied by the liquid phase shrinks during drying whereas the total amount of solute in this volume does not change (precipitation or wall deposit phenomena being assumed negligible). It was shown in [13] that the commonly used continuum model of solute transport [41–43] did not lead to a good agreement with PNM simulations. This was attributed to the fact that the classical approach does not distinguish between the percolating liquid phase and the nonpercolating liquid phase. The objective in what follows is to explore whether the three equation continuum model can help alleviate the discrepancies between the PNM simulations and the continuum approach. To this end, we focus on the second mechanism as regards the variation of the solute concentration. This mechanism is referred to as the liquid phase shrinking effect since the increase in the concentration due to this mechanism results from the decrease in the volume occupied by the liquid phase in the porous medium. We only consider the limiting situation where convective effect on the solute transport can be neglected, i.e., the very low Péclet number case [41]. This corresponds for instance to a very low evaporation rate. This limiting situation is referred to as the hyperdiffusive limit since the solute concentration is consistently assumed to be spatially uniform in each liquid cluster. Therefore, in this limit, there is no need to compute the velocity field in the liquid phase. The solution is dilute so that impact of the solute on the surface tension, the liquid density, or the equilibrium vapor pressure at the menisci can be neglected.

A. PNM computations

Initially, the concentration is uniform in the liquid phase and denoted by C_0. Then the concentration is updated in each cluster according to the mass conservation equation,

$$C_i(t+\delta t)V_i(t+\delta t) = C_i(t)V_i(t), \tag{25}$$

where C_i is the concentration in cluster i and V_i is the volume of liquid cluster i. The time step δt in Eq. (25) is the time step of the PNM drying algorithm. Equation (25) is for a shrinking cluster. A cluster can also split into two smaller clusters as the result of the invasion of a pore by the gas phase. In this case, the concentration $C_{i1} = C_{i2} = C_{i1/i2}$ in the newly formed cluster i_1 and i_2 is computed from the equation

$$C_{i1/i2}(t+\delta t)[V_{i1}(t+\delta t) + V_{i2}(t+\delta t)] = C_i(t)V_i(t), \tag{26}$$

where V_{i1}, V_{i2}, and V_i are the volumes of cluster i_1, i_2, and i respectively.

Then the slice averaged concentrations are computed by volume averaging the concentration in each slice,

$$C_{\text{sl}}(t,z) = \frac{\sum_{i=1}^{i=n} C_i(t)V_{i\text{sl}}(t)}{\sum_{i=1}^{i=n} V_{i\text{sl}}(t)} = \frac{\sum_{i=1}^{i=n} C_i(t)V_{i\text{sl}}(t)}{\varepsilon S_{\text{sl}} Ah}, \tag{27}$$

$$C_{2\text{sl}}(t,z) = \frac{\sum_{i=2}^{i=n} C_{2i}(t)V_{i\text{sl}}(t)}{\sum_{i=2}^{i=n} V_{i\text{sl}}(t)} = \frac{\sum_{i=2}^{i=n} C_{2i}(t)V_{i\text{sl}}(t)}{\varepsilon S_{2\text{sl}} Ah}, \tag{28}$$

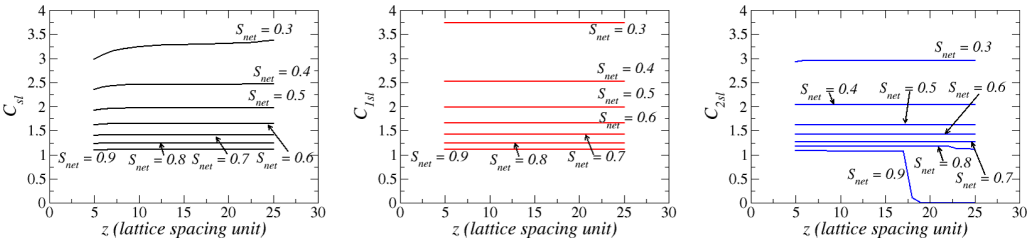

FIG. 9. Profiles of $C_{\rm sl}$, $C_{\rm 1sl}$, and $C_{\rm 2sl}$ in the network corresponding to $S_{\rm net} = 0.9$, 0.8, 0.7, 0.6, 0.5, 0.4, 0.3; $z = 0$ corresponds to the network top surface (Fig. 2) whereas $z = 30$ corresponds to the network bottom limiting surface.

where $V_{i\rm sl}$ is the volume of cluster i present in the considered slice, $h = 10\,a$ is the slice thickness. It is recalled that label 1 is for the percolating cluster. The concentration in the latter is spatially uniform over the whole network. Since C_1 is uniform of the network, it is obvious that the slice averaged concentration $C_{\rm 1sl}$ is spatially uniform and equal to $C_{\rm 1net}$.

The evolution of the three slice average concentration profiles, namely $C_{\rm sl}$, $C_{\rm 1sl}$, and $C_{\rm 2sl}$, during stage 1 is depicted in Fig. 9. As expected the concentration increases during stage 1 because of the liquid cluster dynamics, i.e., the fact that clusters split and shrink. However, it can be noticed that the fragmentation process occurs essentially in the main cluster, i.e., the cluster forming the percolating liquid phase, when only the bulk region is considered since the evaporation rate of the isolated clusters located within the bulk region is quite small (Fig. 8). Interestingly, the concentration profiles are flat. This was of course expected for $C_{\rm 1sl}$ since the concentration is uniform in the percolating liquid phase but somewhat less obvious as regards the nonpercolating liquid phase slice averaged concentration, i.e., $C_{\rm 2sl}$. This point is discussed further below and explained in the discussion section (Sec. VII).

Also, the results shown in Fig. 9 indicate that the concentration is greater in the percolating liquid phase than in the nonpercolating liquid phase and thus greater than the average concentration in the liquid phase. This is better illustrated in Fig. 10 showing the variations of $C_{\rm bulk}$, $C_{\rm 1\,bulk}$, and $C_{\rm 2\,bulk}$. As for the saturations $S_{\rm bulk}$, $S_{\rm 1\,bulk}$, and $S_{\rm 2\,bulk}$, $C_{\rm bulk}$, $C_{\rm 1\,bulk}$, and $C_{\rm 2\,bulk}$ are the averaged concentrations over the slice located at $z = 16$. $C_{\rm bulk}$ is computed as

$$C_{\rm bulk}(t) = \frac{\sum_{i=1}^{i=n} C_i(t) V_{i\rm sl}(t)}{\sum_{i=1}^{i=n} V_{i\rm sl}(t)}, \tag{29}$$

where $i = 1$ is for the percolating cluster and n is the number of liquid clusters present in the considered slice. Similarly, the average solute concentration in the nonpercolating clusters is computed as

$$C_{\rm 2\,bulk} = \frac{\sum_{i=2}^{i=n} C_i(t) V_{i\rm sl}(t)}{\sum_{i=2}^{i=n} V_{i\rm sl}(t)}. \tag{30}$$

Note again that the concentration is uniform over the percolating cluster and therefore the slice concentration $C_{\rm 1\,bulk}$ is equal to the concentration over the whole percolation cluster.

Figure 10 clearly illustrates why it is important to distinguish the percolating and nonpercolating liquid phases. Not making this distinction, as in the commonly used approach, i.e., [41–43], leads to underestimate the concentration and thus for instance to overestimate the time corresponding to the onset of crystallization when C corresponds to a dissolved salt concentration [44]. Then the question arises as to whether the evolution depicted in Fig. 10 can be captured by an extended version of the three equation continuum model considering also the presence of the solute. This is studied in the section that follows.

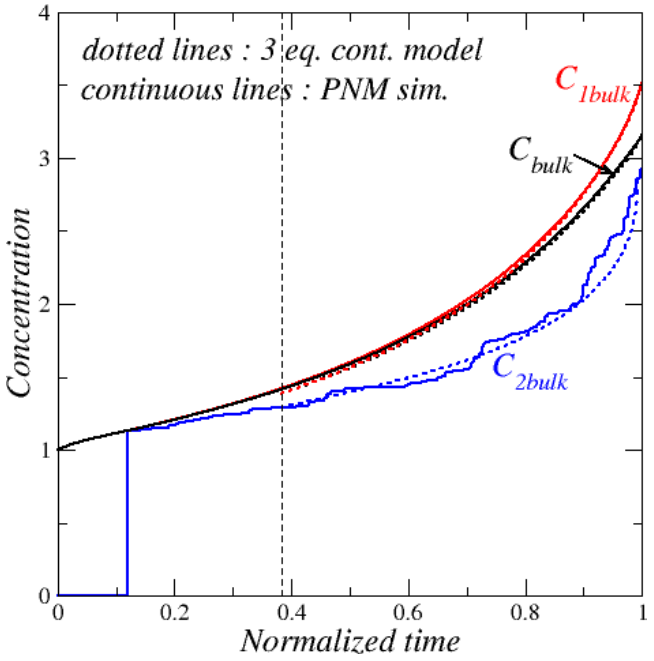

FIG. 10. Variation of C_{bulk}, $C_{1\,\text{bulk}}$, and $C_{2\,\text{bulk}}$ in the network as a function of time during stage 1. The reference time is the time at the end of stage 1 defined as the time when $S_{\text{net}} = 0.31$. The vertical dashed line indicates the beginning of the period of interest for the comparison with the three equation continuum model (see text).

B. Continuum approach

Within the framework of the three equation continuum model, the solute transport equation in the percolating liquid phase is expressed as

$$\varepsilon \frac{\partial S_1 C_1}{\partial t} = \nabla \cdot (\varepsilon S_1 D_{s1}^* \nabla C_1) - \dot{m}_{12s}, \tag{31}$$

where $\dot{m}_{12s}$ (kg/m^3/s) is the solute mass exchange term between the percolating liquid phase and the nonpercolating liquid phase. Equation (31) is similar to the solute transport equation in the classical approach [41–43]. The difference lies in the fact that the considered liquid phase is the percolating liquid phase and not the whole liquid phase.

For the nonpercolating liquid phase, the solute conservation equation is simply expressed as

$$\varepsilon \frac{\partial S_2 C_2}{\partial t} = \dot{m}_{12s} \tag{32}$$

since the convective transport is assumed negligible in the isolated clusters.

Integrating Eqs. (31) and (32) over the porous medium height leads to

$$\varepsilon H_{pm} \frac{\partial S_1 C_1}{\partial t} = -\int_0^{H_{pm}} \dot{m}_{12s} dz, \tag{33}$$

$$\varepsilon H_{pm} \frac{\partial S_2 C_2}{\partial t} = \int_0^{H_{pm}} \dot{m}_{12s} dz. \tag{34}$$

Since the profiles are approximately spatially uniform in the bulk (as shown in Figs. 5 and 9), Eqs. (33) and (34) can be expressed as

$$\varepsilon \frac{\partial S_{1\,\mathrm{bulk}} C_{1\,\mathrm{bulk}}}{\partial t} = -\dot{m}_{12s}, \tag{35}$$

$$\varepsilon \frac{\partial S_{2\,\mathrm{bulk}} C_{2\,\mathrm{bulk}}}{\partial t} = \dot{m}_{12s}. \tag{36}$$

The exchange term $\dot{m}_{12s}$ in Eqs. (35) and (36) is modeled using an expression similar to the one for $\dot{m}_{12}$ since the solute mass transfer between the percolating liquid phase and the nonpercolating liquid phase is due to clusters separating from the main cluster. Furthermore, since the solute concentration in the main cluster is C_1 it is reasonable to consider that $\dot{m}_{12s}$ should be proportional to C_1. This finally leads us to express $\dot{m}_{12s}$ as

$$-\dot{m}_{12s} = \eta \varepsilon C_{1\,\mathrm{bulk}} \left(\frac{S_{2\,\mathrm{bulk}} - S_{\mathrm{irr}}}{S_{\mathrm{irr}} - S_{\mathrm{bulk}}} \right) \frac{\partial S_{\mathrm{bulk}}}{\partial t}. \tag{37}$$

Equations (35) and (36) combined with Eq. (37) were solved using a method similar to the one used for solving Eqs. (22) and (23) with, as for the saturation problem , $\eta = 0.1$ and $S_{\mathrm{irr}} = 0.3138$. A first order finite difference scheme to express the derivatives with respect to time was used, i.e., expressions of the form $\frac{\partial S_{1\,\mathrm{bulk}} C_{1\,\mathrm{bulk}}}{\partial t} = \frac{(S_{1\,\mathrm{bulk}} C_{1\,\mathrm{bulk}})(t+\delta t) - (S_{1\,\mathrm{bulk}} C_{1\,\mathrm{bulk}})(t)}{\delta t}$. The method was explicit, i.e., the values of the saturations and the value of $C_{1\,\mathrm{bulk}}$ involved in the expression of the source term $\dot{m}_{12s}$ were taken at the previous time step. Then $S_{\mathrm{bulk}} C_{\mathrm{bulk}}$ was obtained from $S_{\mathrm{bulk}} C_{\mathrm{bulk}} = S_{1\,\mathrm{bulk}} C_{1\,\mathrm{bulk}} + S_{2\,\mathrm{bulk}} C_{2\,\mathrm{bulk}}$.

This led to the results depicted in Fig. 11. As can be seen, the three equation continuum model leads here again to a quite reasonably good agreement with the PNM data. As explained before, only the range of saturations not significantly affected by the initial finite size effect is considered for the comparison between the continuum model and the PNM data. This corresponds to the overall network saturations lower than approximately $S_{\mathrm{net}} = 0.7$. The time corresponding to $S_{\mathrm{net}} = 0.7$ is indicated by a vertical dashed line in Fig. 11.

As expected, the product $S_{\mathrm{bulk}} C_{\mathrm{bulk}}$ is constant over the period of interest. This simply means that the total mass of solute in the bulk region is conserved. The total mass of solute in the percolating phase, i.e., $S_{1\,\mathrm{bulk}} C_{1\,\mathrm{bulk}}$, decreases. This is because the percolating liquid phase loses mass as the result of the fragmentation process. The corresponding mass loss corresponds to the mass of solute gained by the nonpercolating liquid phase, which therefore increases during stage 1. The latter corresponds to $S_{2\,\mathrm{bulk}} C_{2\,\mathrm{bulk}}$ in Fig. 11.

From the computation of $S_{\mathrm{bulk}} C_{\mathrm{bulk}}$, $S_{1\,\mathrm{bulk}} C_{1\,\mathrm{bulk}}$, and $S_{2\,\mathrm{bulk}} C_{2\,\mathrm{bulk}}$ depicted in Fig. 11 and the computation of S_{bulk}, $S_{1\,\mathrm{bulk}}$, and $S_{2\,\mathrm{bulk}}$ depicted in Fig. 7, the solute concentrations C_{bulk}, $C_{1\,\mathrm{bulk}}$, and $C_{2\,\mathrm{bulk}}$ were obtained as $C_{\mathrm{bulk}} = \frac{S_{\mathrm{bulk}} C_{\mathrm{bulk}}}{S_{\mathrm{bulk}}}$, $C_{1\,\mathrm{bulk}} = \frac{S_{1\,\mathrm{bulk}} C_{1\,\mathrm{bulk}}}{S_{1\,\mathrm{bulk}}}$, and $C_{2\,\mathrm{bulk}} = \frac{S_{2\,\mathrm{bulk}} C_{2\,\mathrm{bulk}}}{S_{2\,\mathrm{bulk}}}$. The corresponding results are compared to the PNM simulation data in Fig. 10. As can be seen, the three equation continuum model predicts quite well the variations of the three considered solute concentrations. In particular, the important fact that the solute concentration is greater in the percolating liquid phase is well captured.

VII. DISCUSSION

The classical one equation continuum model [41–43] predicts that the solute concentration is uniform over the liquid phase in the considered very low Péclet number limit during stage 1. This solute concentration is simply given by

$$C(t) = \frac{S_{\mathrm{net}0} C_0}{S_{\mathrm{net}}(t)}, \tag{38}$$

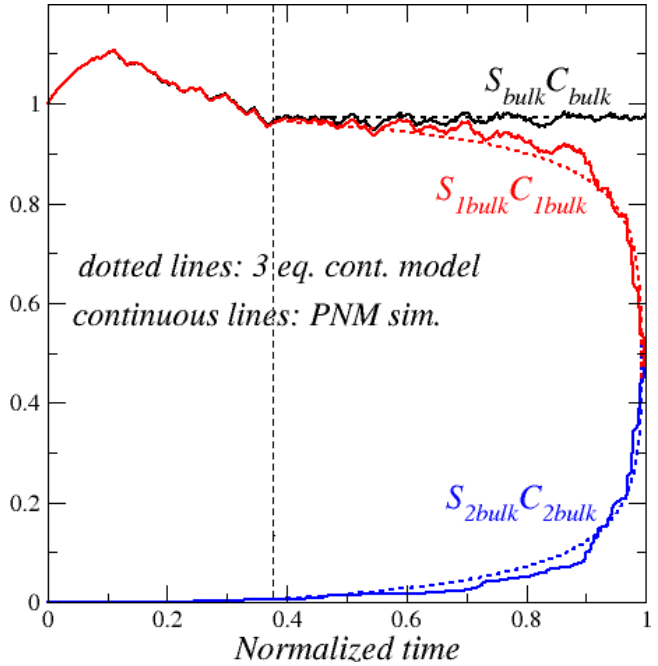

FIG. 11. Variation of $S_{\text{bulk}}C_{\text{bulk}}$, $S_{1\,\text{bulk}}C_{1\,\text{bulk}}$, and $S_{2\,\text{bulk}}C_{2\,\text{bulk}}$ in the network as a function of time during stage 1. The reference time is the time at the end of stage 1 defined as the time when $S_{\text{net}} = 0.31$. The vertical dashed line corresponds to the time when $S_{\text{net}} = 0.7$ (as explained in the text, only the times greater than the time corresponding to $S_{\text{net}} = 0.7$ are considered for the comparison between the continuum model and the PNM data).

where S_{net0} and C_0 are the initial saturation and solute concentration in the network respectively. $C(t)$ corresponds to C_{bulk} in the results presented in the previous section. The results presented in the previous section clearly show that the solute concentration predicted by this quite classical model in the very low Péclet number limit should not be understood as the solute concentration all over the liquid. The liquid phase is actually fragmented and the solute concentration can vary from one liquid cluster to another. As a result, the solute concentration computed with the classical model must be interpreted as an average concentration over the various liquid clusters, more exactly as a weighted average concentration where the weights are the cluster volume fractions, i.e.,

$$\langle C \rangle = \frac{\sum_{i=1}^{i=n} V_i C_i}{\sum_{i=1}^{i=n} V_i} = \sum_{i=1}^{i=n} \left(\frac{V_i}{\sum_{i=1}^{i=n} V_i} \right) C_i, \tag{39}$$

where V_i is the volume of liquid cluster i and C_i is the solute concentration in cluster i, and n is the number of liquid clusters at the considered time.

In other words, although diffusion is the dominant transport mechanism in the very low Péclet number limit, this does not mean that the solute concentration is spatially uniform in the liquid phase. To illustrate this feature further, the standard deviation of the solute concentration over the various clusters can be computed from the PNM results. Since the percolating and the nonpercolating liquid phases are distinguished with the three equation continuum model, the spatial variability of the solute concentration is illustrated considering the nonpercolating liquid phase. The average

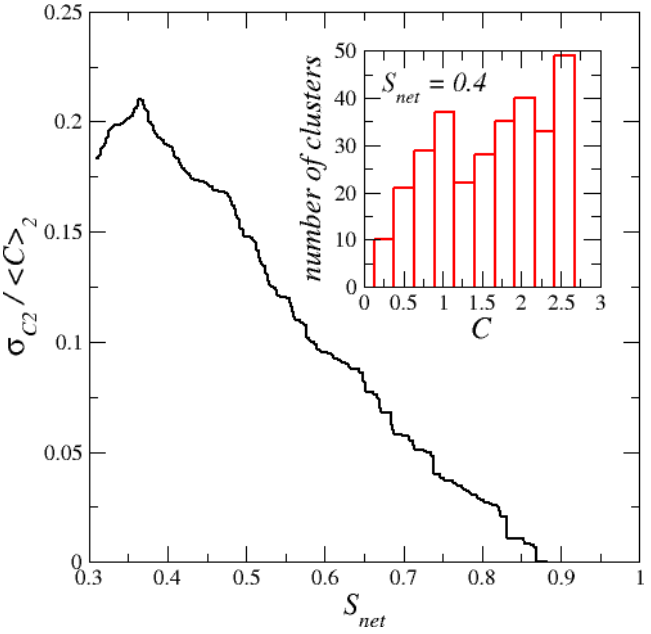

FIG. 12. Variation of the standard deviation σ_{c2} relative to the mean of the solute concentration distribution in the nonpercolating liquid phase over the network bulk region during stage 1. The inset shows the distribution of the concentration in the isolated clusters for $S_{\text{net}} = 0.4$.

solute concentration in the nonpercolating liquid phase is computed as

$$\langle C\rangle_2 = \frac{\sum_{i=2}^{i=n} V_i C_i}{\sum_{i=2}^{i=n} V_i} = \sum_{i=2}^{i=n} \left(\frac{V_i}{\sum_{i=2}^{i=n} V_i} \right) C_i, \tag{40}$$

noting that $i = 1$ corresponds to the main cluster. Thus i in the range $[2, n]$ corresponds to the isolated clusters ($n - 1$ is thus the total number of isolated clusters). The standard deviation of the solute concentration over the nonpercolating liquid phase is then computed as

$$\sigma_{c2} = \sqrt{\frac{\sum_{i=2}^{i=n} V_i (C_i - \langle C\rangle_2)^2}{\sum_{i=2}^{i=n} V_i}}. \tag{41}$$

The variation of σ_{c2} over stage 1 is shown in Fig. 12.

As can be seen, the standard deviation relative to the mean increases during most of stage 1. The decrease toward the end of stage 1 is due to the fact that the mean increases faster than the standard deviation because of the formation of many clusters of higher concentration toward the end of stage 1 (Fig. 4). As illustrated in the inset in Fig. 12, the variation of the solute concentration over the nonpercolating liquid phase is significant with about a factor 2 between the concentration in the clusters of lowest concentration and the clusters of highest concentrations.

The existence of the concentration spatial variability in the considered diffusion dominant regime is directly due to the fact that isolated clusters form from the main cluster all along stage 1 (as illustrated in Fig. 4). The concentration in an isolated cluster in the bulk region is the concentration in the main cluster at the time when the isolated cluster forms. Since the concentration in the main cluster increases during stage 1 (Fig. 11), the later an isolated cluster forms in the bulk region, the greater its concentration is. Based on the main cluster concentration variations depicted in Fig. 11, it can be readily inferred that the concentration over the nonpercolating phase varies at a given time in the range $[C_0, C_1(t)]$.

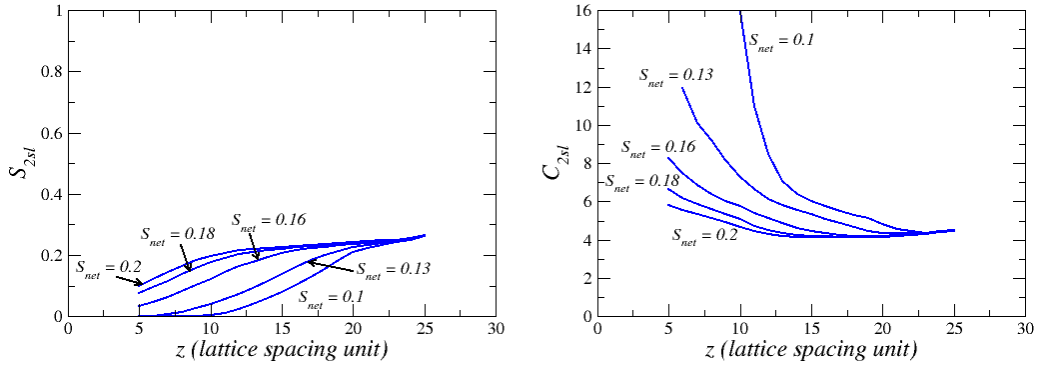

FIG. 13. Evolution of saturation and concentration profiles in stage 2; $z = 0$ corresponds to the network top surface (Fig. 2) whereas $z = 30$ corresponds to the network bottom limiting surface.

However, this spatial variability due to the historicity of the isolated clusters formation from the main cluster does not imply a spatial variation along the network depth. As illustrated in Fig. 9, the mean concentration profiles are flat. This is due to the fact that the probability of forming a new cluster from the main cluster in the bulk region does not depend of the position [20].

The fragmentation of the liquid phase in isolated clusters also leads to a somewhat counterintuitive result after stage 1, i.e., in stage 2. As described in [9], the percolating liquid phase disappears at the end of stage 1 in the considered "asymptotic" regime purely controlled by capillary effects. This regime is described as asymptotic because it is rarely observed in the standard laboratory experiments due to the viscous effects. In most experiments, the liquid phase is actually percolating up to the receding front forming the lower edge of the dry region developing in the network during stage 2. By contrast, in the considered asymptotic regime, the liquid phase is formed by isolated clusters only and the development of the dry zone results from the gradual evaporation of the isolated clusters [9]. This asymptotic regime is expected when evaporation is quite low and/or with sufficiently thin systems. In the considered very low Péclet number limit, the concentration profiles could be expected to be flat due to the dominant diffusion transport in the liquid phase.

However, since the isolated cluster evaporation dynamics is not spatially uniform during stage 2, the concentration profiles are actually not flat. This is illustrated in Fig. 13. The evaporation rate at the boundary of the isolated clusters is significantly greater for the clusters in contact with the dry zone. In other words, the cluster evaporation rate rapidly decreases with the increasing depth in the network. Since the concentration increase is due to the clusters shrinking, the concentration increases faster in the region where the cluster evaporation rate is greater. This leads to the remarkably nonlinear concentration variations depicted in Fig. 13. Interestingly, the concentration profiles roughly tend to resemble the exponential like profiles typically resulting from the competition between advection and diffusion effects [41]. The mechanism leading to the strongly nonlinear shape is of course completely different here and is due to the combination of the fragmentation of the liquid phase in isolated clusters and the screening of the evaporation at the boundary of the clusters located deeper in the network. One can refer to [12] for more details on the screening phenomenon. The screening phenomenon during stage 1 is illustrated in Fig. 8. A similar rapid decrease in the evaporation flux with the distance from the interface between the dry zone and the shrinking liquid cluster zone exists during stage 2.

Since it has been shown that the liquid films can have a strong impact in drying [34,35,45,46], it must be clear that the results presented in this article as regards the solute distribution are for the situations where the impact of the films on the solute distribution is negligible. For instance, it has been shown [47] that the contact angle for an aqueous solution in the presence of a dissolved salt can be relatively high, on the order of 40° or more. With such values of the contact angle,

the development of corner films is significantly hampered. By contrast, for significantly lower contact angles, when the liquid films can develop so as to maintain a hydraulic connection between the "isolated" clusters, some solute transport can occur through the films. This should reduce the concentration variation between clusters. In the case of a sufficiently low evaporation rate for the solute distribution to reach a quasisteady state during drying, solute diffusion in the films might even lead to a uniform concentration distribution all over the liquid phase. Hence, as for the drying process in general, i.e., [45], the consideration of liquid films within the framework of the three equation continuum model would deserve to be studied.

Although the whole set of equations of the three equation continuum model was presented, only a rather simple situation, allowing solving the model quite easily without resorting to the determination of the various transport parameters of the model, was considered. In this respect, it would be interesting to extend the present work by developing a numerical procedure allowing solving the full set of equations. This would notably permit us to simulate the full drying process and not only stage 1 and to consider other regimes than the capillary regime and the very low Péclet number regime.

Also, the edge regions, especially the top edge region in the considered drying configuration, were not studied on the ground that this is the bulk region which is of primary interest for evaluating the continuum models. However, the top region can be of special interest for predicting or analyzing certain phenomena, such as the formation of salt efflorescence at the evaporative surface of porous media for instance, e.g., [36,40,44,48,49]. Thus, some works should be dedicated to the modeling of the transfers in the top edge region in the future.

It can be also noted that a structured cubic pore network was considered in the present paper whereas realistic networks, extracted from microstructure digital images, for instance [50], are unstructured. However, this should not affect the main results of the present paper since the fragmentation process is a general feature inherent to the invasion percolation process at the core of the drying process. The main impact should be on the coefficient η [Eq. (13)] since the value of this coefficient depends on the particular porous medium considered. Considering various networks, i.e., various microstructures, would be interesting to better characterize this coefficient.

VIII. CONCLUSION

A continuum model of drying in capillary porous media, referred to as the three equation continuum model, was presented. Contrary to the commonly used continuum models of drying, the present model makes an explicit distinction between the percolating and nonpercolating liquid phases. From the consideration of the frequently encountered capillary regime, it has been shown that the model was able to predict the variations of the saturation in both the percolating and nonpercolating liquid phases during stage 1. Then, the model was extended so as to predict the evolution of the concentration of a solute in both the percolating and nonpercolating liquid phases. Comparisons with data obtained from pore network simulations were quite satisfactory. In particular, the continuum model consistently predicts that the solute concentration is higher in the percolating phase than in the nonpercolating phase. However, only the very low Péclet number regime was considered.

Nevertheless, the results presented in this article also clarify the meaning of the solute concentration predicted by the continuum models, which should be considered as an average concentration over the fragmented liquid phase. Counterintuitively, it has been shown that the concentration is not necessarily uniform over the liquid phase in the considered very low Péclet number regime. As the result of the liquid fragmentation in numerous clusters, spatial fluctuations of the concentration are expected even in the very low Péclet number limit.

In summary, the three equation continuum model allows significantly more accurate predictions of the solute distribution during drying compared to the classical one equation model. In the more general context of the macroscopic theory of biphasic flow in porous media, the present paper presents both an extension to drying, with and without the presence of a solute, of the

model proposed in [15–18] and an additional validation of this model, in particular as regards the formulation of the mass exchange term between the percolating and nonpercolating liquid phases.

ACKNOWLEDGMENTS

Financial support from joint project "Drycap" funded by GIP ANR (Project No. 16-CE92-0030-01) and DFG (Project No. TS28/10-1) is gratefully acknowledged.

[1] A. S. Mujumdar, *Handbook of Industrial Drying*, 4th ed. (CRC, Boca Raton, 2015).
[2] H. Ito, K. Abe, M. Ishida, A. Nakano, T. Maeda, T. Munakata, H. Nakajima, and T. Kitahara, Effect of through-plane distribution of polytetrafluoroethylene in carbon paper on in-plane gas permeability, J. Power Sources **248**, 822 (2014).
[3] C. Kumar, M. A. Karim, and M. U. H. Joardder, Intermittent drying of food products: A critical review, J. Food Eng. **121**, 48 (2014).
[4] C. Villani, R. Spragg, M. Pour-Ghaz, and W. J. Weiss, The Influence of pore solutions properties on drying in cementitious materials, J. Am. Ceram. Soc. **97**, 386 (2014).
[5] D. Or, P. Lehmann, E. Shahraeeni, and N. Shokri, Advances in soil evaporation physics—A review, Vadose Zone J. **12**, 1 (2013).
[6] S. Whitaker, Simultaneous heat, mass and momentum transfer in porous media. A theory of drying, in *Advances in Heat Transfer* (Academic, New York, 1977), Vol. 13, pp. 119–203.
[7] H. T. Vu and E. Tsotsas, Mass and heat transport models for analysis of the drying process in porous media: A review and numerical implementation, Int. J. Chem. Eng. **2018**, 9456418 (2018).
[8] L. Pel, K. A. Landman, and E. F. Kaasschierter, Analytic solution for the non-linear drying problem, Int. J. Heat Mass Transfer **45**, 3173 (2002).
[9] Y. Le Bray and M. Prat, Three-dimensional pore network simulation of drying in capillary porous media, Int. J. Heat Mass Transfer **42**, 4207 (1999).
[10] D. Wilkinson and J. F. Willemsen, Invasion percolation: A new form of percolation theory, J. Phys. A: Math. Gen. **16**, 3365 (1983).
[11] M. Prat, Percolation model of drying under isothermal conditions in porous media, Int. J. Multiphase Flow **19**, 691(1993).
[12] M. Prat, Isothermal drying of non-hygroscopic capillary-porous materials as an invasion percolation process, Int. J. Multiphase Flow **21**, 875 (1995).
[13] F. Ahmad, A. Rahimi, E. Tsotsas, M. Prat, and A. Kharaghani, From micro-scale to macro-scale modeling of solute transport in drying capillary porous media, Int. J. Heat Mass Transfer **165**, 120722 (2021).
[14] E. Keita, P. Faure, S. Rodts, and P. Coussot, MRI evidence for a receding-front effect in drying porous media, Phys. Rev. E **87**, 062303 (2013).
[15] R. Hilfer, Capillary pressure, hysteresis and residual saturation in porous media, Phys. A (Amsterdam, Neth.) **359**, 119 (2006).
[16] R. Hilfer, Macroscopic capillarity without a constitutive capillary pressure function, Phys. A (Amsterdam, Neth.) **371**, 209 (2006).
[17] R. Hilfer, Macroscopic capillarity and hysteresis for flow in porous media, Phys. Rev. E **73**, 016307 (2006).
[18] F. Doster, P. A. Zegeling, and R. Hilfer, Numerical solutions of a generalized theory for macroscopic capillarity, Phys. Rev. E **81**, 036307 (2010).
[19] A. Attari Moghaddam, M. Prat, E. Tsotsas, and A. Kharaghani, Evaporation in capillary porous media at the perfect piston-like invasion limit: Evidence of nonlocal equilibrium effects, Water Resour. Res. **53**, 10433 (2017).
[20] A. Attari Moghaddam, A. Kharaghani, E. Tsotsas, and M. Prat, Kinematics in a slowly drying porous medium: Reconciliation of pore network simulations and continuum modeling, Phys. Fluids **29**, 022102 (2017).

[21] F. Ahmad, M. Talbi, M. Prat, E. Tsotsas, and A. Kharaghani, Non-local equilibrium continuum modeling of partially saturated drying porous media: Comparison with pore network simulations, Chem. Eng. Sci. **228**, 115957 (2020).
[22] A. G. Yiotis, I. N. Tsimpanogiannis, A. K. Stubos, and Y. C. Yortsos, Pore-network study of the characteristic periods in the drying of porous materials, J. Colloid Interface Sci. **297**, 738 (2006).
[23] E. F. Medici, I. V. Zenyuk, D. Y. Parkinson, A. Z. Weber, and J. S. Allen, Understanding water transport in polymer electrolyte fuel cells using coupled continuum and pore-network models, Fuel Cells **16**, 725 (2016).
[24] N. Belgacem, M. Prat, and J. Pauchet, Coupled continuum and condensation-evaporation pore network model of the cathode in polymer-electrolyte fuel cell, Int. J. Hydrogen Energy **42**, 8150 (2017).
[25] F. Nandjou, J.-P. Poirot-Crouvezier, M. Chandesris, and Y. Bultel, A pseudo-3D model to investigate heat and water transport in large area PEM fuel cells–Part 1: Model development and validation, Int. J. Hydrogen Energy **41**, 15545 (2016).
[26] J. van Brakel, Mass transfer in convective drying, in *Advances in Drying*, edited by A. S. Mujumdar (Hemisphere, New York, 1980), pp. 217–267.
[27] W. Brutsaert and D. Chen, Desorption and the two stages of drying of natural tallgrass prairie, Water Resour. Res. **31**, 1305 (1995).
[28] A. Attari Moghaddam, A. Kharaghani, E. Tsotsas, and M. Prat, A pore network study of evaporation from the surface of a drying non-hygroscopic porous medium, AIChE J. **64**, 1435 (2018).
[29] M. Talbi and M. Prat, About Schlünder's model: A numerical study of evaporation from partially wet surfaces, Drying Technol. **37**, 513 (2019).
[30] M. Talbi and M. Prat, Coupling between internal and external mass transfer during stage 1 evaporation in capillary porous media: Interfacial resistance approach, Phys. Rev. E **104**, 055102 (2021).
[31] M. Prat, Recent advances in pore-scale models for drying of porous media, Chem. Eng. J. **86**, 153 (2002).
[32] M. Prat, Pore network models of drying, contact angle and films flows, Chem. Eng. Technol. **34**, 1029 (2011).
[33] T. Metzger, E. Tsotsas, and M. Prat, Pore-network models: A powerful tool to study drying at the pore level and understand the influence of structure on drying kinetics, in *Computational Tools at Different Scales*, Modern Drying Technology Vol. 1, edited by A. Mujumdar and E. Tsotsas (Wiley, New York, 2007), Chap. 2, pp. 57–102.
[34] M. Prat, On the influence of pore shape, contact angle and film flows on drying of capillary porous media, Int. J. Heat Mass Transfer **50**, 1455 (2007).
[35] F. Chauvet, P. Duru, S. Geoffroy, and M. Prat, Three Periods of Drying of a Single Square Capillary Tube, Phys. Rev. Lett. **103**, 124502 (2009).
[36] S. Gupta, H. P. Huinink, M. Prat, L. Pel, and K. Kopinga, Paradoxical drying due to salt crystallization, Chem. Eng. Sci. **109**, 204 (2014).
[37] J. Thiery, S. Rodts, D. A. Weitz, and P. Coussot, Drying regimes in homogeneous porous media from macro- to nanoscale, Phys. Rev. Fluids **2**, 074201 (2017).
[38] D. Stauffer and A. Aharony, *Introduction to Percolation Theory* (Taylor & Francis, London, 1992).
[39] X. Lu, A. Kharaghani, and E. Tsotsas, Transport parameters of macroscopic continuum model determined from discrete pore network simulations of drying porous media, Chem. Eng. Sci. **223**, 115723 (2020).
[40] B. Diouf, S. Geoffroy, A. Abou-Chakra, and M. Prat, Locus of first crystals on the evaporative surface of a vertically textured porous medium, EPJ Appl. Phys. **81**, 11102 (2018).
[41] H. P. Huinink, L. Pel, and M. A. J. Michels, How ions distribute in a drying porous medium: A simple model, Phys. Fluids **14**, 1389 (2002).
[42] L. Guglielmini, A. Gontcharov, A. J. Aldykiewicz, and H. A. Stone, Drying of salt solutions in porous materials: Intermediate-time dynamics and efflorescence, Phys. Fluids **20**, 077101 (2008).
[43] N. Sghaier, M. Prat, and S. Ben Nasrallah, On ions transport during drying in a porous medium, Transp. Porous Media **67**, 243 (2007).
[44] F. Hidri, N. Sghaier, H. Eloukabi, M. Prat, and S. Ben Nasrallah, Porous medium coffee ring effect and other factors affecting the first crystallisation time of sodium chloride at the surface of a drying porous medium, Phys. Fluids **25**, 127101 (2013).

[45] A. G. Yiotis, A. G. Boudouvis, A. K. Stubos, I. N. Tsimpanogiannis, and Y. C. Yortsos, Effect of liquid films on the drying of porous media, AIChE J. **50**, 2721 (2004).

[46] A. G. Yiotis, D. Salin, E. S. Tajerand, and Y. C. Yortsos, Drying in porous media with gravity-stabilized fronts: Experimental results, Phys. Rev. E **86**, 026310 (2012).

[47] N. Sghaier, M. Prat, and S. Ben Nasrallah, On the influence of sodium chloride concentration on equilibrium contact angle, Chem. Eng. J. **122**, 47 (2006).

[48] H. Eloukabi, N. Sghaier, S. Ben Nasrallah, and M. Prat, Experimental study of the effect of sodium chloride on drying of porous media: The crusty-patchy efflorescence transition, Int. J. Heat Mass Transfer **56**, 80 (2013).

[49] J. Desarnaud, H. Derluyn, L. Molari, S. de Miranda, V. Cnudde, and N. Shahidzadeh, Drying of salt contaminated porous media: Effect of primary and secondary nucleation, J. Appl. Phys. **118**, 114901 (2015).

[50] H. Dong and M. J. Blunt, Pore-network extraction from micro-computerized-tomography images, Phys. Rev. E **80**, 036307 (2009).